Development of a Robotic Hummingbird Capable of Controlled Hover




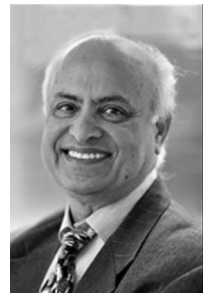

David Coleman*
Graduate Student

Moble Benedict
Assistant Professor

Texas A&M University, College Station, TX

Vikram Hirishikeshaven
Assistant Research Scientist

Inderjit Chopra
Alfred Gessow Rotorcraft Center Director

University of Maryland, College Park, MD

This paper details the design, development, and flight testing of a 62-g hummingbird-inspired flapping wing micro air vehicle with hovering capability. The key barriers overcome in the development of this vehicle included optimizing the wing design via aeroelastic tailoring techniques, designing insect-based wing kinematic modulation mechanisms for control and stabilization, trimming, and implementing feedback control during flight. Additionally, a five-bar linkage system was developed to generate large flap-stroke amplitudes, and thus sufficient lift for hover at moderate flapping frequencies (∼25 Hz). Systematic experimental studies were utilized to design lightweight (∼0.8 g) flexible wings, and a fabrication technique was developed to ensure that the wings could be reproduced consistently. The wing kinematic modulation mechanisms, which change the magnitude and direction of the lift vectors during flight, are controlled via a custom-built kinematic autopilot that senses the vehicle dynamics and transmits corrective signals to the mechanism actuators. This has led to several flight experiments in which the vehicle has successfully demonstrated stability and hover capability.

Nomenclature

d	vertical distance from wing aerodynamic center to vehicle center of gravity, mm
f	flapping frequency, Hz
H_L	horizontal component of the left wing lift vector, N
H_R	horizontal component of the right wing lift vector, N
L	left wing
L_L	left wing lift vector, N
L_R	right wing lift vector, N
l_{ext}	extension of link 4 beyond the pivot point, mm
l_R	length of roll trim link in modified five-bar mechanism, mm
l_1	length of link 1 in four-bar mechanism, mm
l_2	length of link 2 in four-bar mechanism, mm
l_3	length of link 3 in four-bar mechanism, mm
l_4	length of link 4 in four-bar mechanism, mm
l_5	length of link 5 in modified five-bar mechanism, mm
R	right wing
V_L	vertical component of left wing lift vector, N
V_R	vertical component of right wing lift vector, N
β_L	tilt angle of left wing-flapping plane, deg
β_R	tilt angle of right wing-flapping plane, deg
ζ_L	left wing flap stroke amplitude, deg
ζ_R	right wing flap stroke amplitude, deg
θ_c	complementary angle of θ_4: $\pi/2 - \theta_4$, deg
θ_2	outside angle of link 2 in four-bar mechanism, deg
θ_3	inside angle of link 3 in four-bar mechanism, deg
θ_4	inside angle of link 4 in four-bar mechanism, deg
θ_5	outside angle of link 5 in modified five-bar mechanism, deg

*Corresponding author; e-mail: dcaero14@tamu.edu.

This paper was presented at the AHS International 71st Annual Forum, Virginia Beach, VA, May 5–7, 2015. Additionally, this paper was runner up for the Robert L. Lichten award. Manuscript received August 2015; accepted November 2016.

Introduction

It is quite fascinating to study Octave Chunate's *Progress in Flying Machines* published in 1894 and examine the many bizarre human-powered "flying" devices that attempted to replicate the graceful flapping flight of biological flyers (Ref. 1). Each concept that emerged grew stranger, with its inventor ever hopeful that his machine would elegantly take to the air like a bird. Ultimately, every one of these devices failed due to a lack of understanding of the fundamentals of flapping wing flight, including aerodynamics and thrust requirements, as well as the need for excellent power-to-weight- and strength-to-weight-ratio systems. It has only been the recent advent of micro air vehicles (MAVs) that has made flying using flapping wings a reality. Useful as aerial surveillance vehicles, MAVs are constructed utilizing the latest advances in lightweight composites, microelectronics, and batteries, enabling designers to miniaturize the vehicles down to an acceptable size for flapping flight mimicking that of a hummingbird. Importantly, biological flapping wing flight offers superior maneuverability, gust tolerance, and disturbance rejection capabilities (Ref. 2). This could be because flapping wing aerodynamics involves several unsteady phenomena (such as leading edge vortices) at low Reynolds numbers that significantly enhance lift production (Ref. 3). Extensive computational and experimental work further support the presence of lift coefficients on flapping wings much higher than that experienced by rotors and fixed wings (Refs. 4, 5).

A few successful flapping-wing MAVs have been built and flown recently. The most notable ones include the DelFly from Delft University

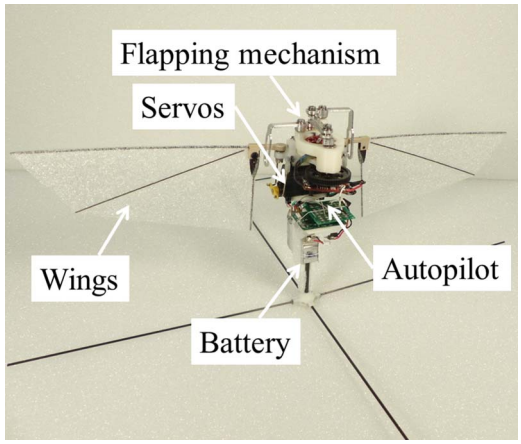

Fig. 1. Hover-capable flapping wing MAV with a mass of 62 g.

(Ref. 6), the Techject developed initially at Georgia Tech (Ref. 7), the RoboRaven at the University of Maryland (Ref. 8), the RoboBee from Harvard University (Ref. 9), the Smartbird built by Festo (Ref. 10), and the Nano Hummingbird by AeroVironment (Ref. 11). It is important to note several characteristics of these vehicles, however, which limit their similarity with hovering biological flyers. Both the RoboRaven and Smartbird, like most flapping wing MAVs, are ornithopters and therefore must rely on forward speed to stay aloft. Both the DelFly and Techject have four wings instead of two, with the DelFly being outfitted with several external control surfaces very much unlike natural flyers. Furthermore, the RoboBee, while capable of hover, must be tethered to the ground to power its piezoelectric benders. This leaves the Nano Hummingbird, a much more biomimetic flyer with a mass of 19 g. This vehicle is prohibitively costly due to its mechanical complexity, is quite small with limited payload capability, and achieves control through varying the wing properties instead of, like biological flyers, through wing kinematics variation. The goal, therefore, of the present study is to design and build a truly biologically inspired two-winged hover-capable MAV with mechanical simplicity that implements wing kinematic modulation methods for control (Fig. 1). Furthermore, this study focuses on developing a vehicle for the purpose of experimentally understanding the aeromechanics, flight dynamics, and controllability of hovering flight similar to that of an insect or hummingbird. The current vehicle prototype has a 30-cm wingspan, flaps at about 21 Hz, and has a mass of 62 g, heavier than even the "Giant hummingbird," the world's heaviest hummingbird (Refs. 12, 13). To calculate the Reynolds number at which the present MAV operates, it is possible to use a concise relationship from Ref. 14 relating the wing length, flapping frequency, and flap amplitude:

$$Re = \frac{4\zeta_L f R_w^2}{\nu AR} \tag{1}$$

Here, the nominal amplitude of the left wing $\zeta_L = 110$ deg, the flapping frequency $f = 21$ Hz, the wing length $R_W = 14$ cm, the aspect ratio $AR = 3.7$, and the kinematic viscosity of air $\nu = 1.48 \times 10^{-5}$ m^2/s. Using these parameters, the Reynolds number for this vehicle is $Re = 5.8 \times 10^4$ at operational conditions. This is at the lower end of the bird and represents an MAV flight regime. By comparison, the Nano Hummingbird has a Reynolds number slightly lower at $Re = 4.0 \times 10^4$, primarily because the wingspan is only slightly more than half of the wingspan of the present vehicle.

The following sections outline in detail the design and development of the wings, flapping mechanism for large amplitude generation, and wing kinematic modulation mechanisms for stability and control. Using a custom-built kinematic autopilot with closed loop control, the vehicle has been flown successfully, and the results of these flight tests are presented as well.

Table 1. Component weight breakdown

Component	Mass (g)	% Total
Wings	1.7	2.7
Motor + flap mechanism	16.7	26.9
Actuators + mechanisms	16.8	27.0
Fuselage/structure	9.5	15.3
Electronics	7.0	11.3
Battery	10.4	16.8
Total	62.1	100

Vehicle Design

The primary concern in the design and development of the present vehicle is its gross weight; therefore, effort was made continuously to reduce the weight of each of the components while maintaining the necessary strength to withstand the large forces imposed during flapping. For this reason, every load-bearing structural component was designed to have a high strength-to-weight ratio. The main body of the vehicle, with a mass of only 4.3 g, functions as an anchor point for all the mechanical subsystems (motor, flapping mechanism, actuators, and wing kinematic modulation mechanisms), is rapid prototyped out of a low-density nylon-based material with exceptional strength. Using specially designed arches and reinforcements at stress concentration points, it is engineered to be as light as possible while maintaining the necessary structural integrity for high-amplitude dynamic loads. A 2.75-mm-diameter carbon fiber rod extends from the main body downward to support the remainder of the vehicle subsystems: the electronics, battery pack, and landing gear. A weight breakdown of the vehicle components is provided in Table 1. Designing each of these components for optimal performance was critical to ensure successful vehicle operation. The subsequent subsections describe the development of the key subsystem components in detail.

Wing drive mechanism

For the present vehicle, the goal was to increase the stroke amplitude as much as possible to reduce the disk loading and also to lower the required operational frequency. An investigation into the methods used by other flapping wing vehicle designers shows that there is a lack of a simple and elegant solution to this problem. Traditionally, four-bar mechanisms are employed (Refs. 6,8,10,15); however, owing to the maximum angle limitations of the four-bar mechanism, it is not applicable for truly hovering flight. The Nano Hummingbird generates 180 deg of flapping motion, via a complex string and pulley system (Ref. 11). Some designers have placed a spring in serial with the main wing spar; however, it is difficult to tune the resonant frequency of the spring to the operational flapping frequency (Ref. 16). Therefore, to obtain large flapping amplitudes for the present vehicle, a simple, yet novel mechanism consisting of a traditional four linkage system with an added "fifth" bar and slider, which amplifies the output from the four-bar mechanism was developed (Ref. 17). This is shown in a photograph in Fig. 2(a), and schematically in Fig. 2(b). The traditional four-bar crank-rocker mechanism converts motor rotation into reciprocating flapping motion with approximately ±20 deg of stroke amplitude. A close-up schematic of the left wing four-bar mechanism is shown in Fig. 3, where l_4 and θ_4 are the output bar and its angle, respectively. The fifth bar portion of the mechanism

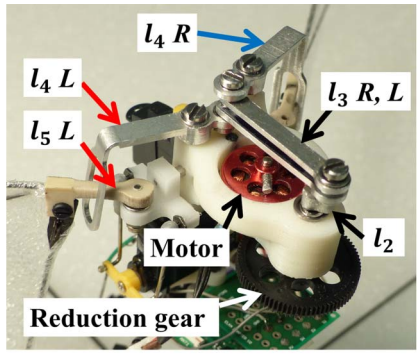

(a)

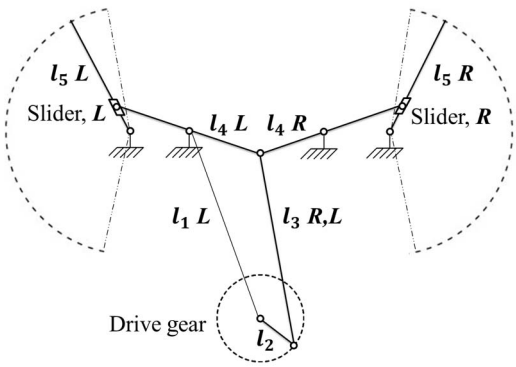

(b)

Fig. 2. (a) Modified five-bar mechanism implemented on the vehicle. (b) Schematic of complete modified five-bar mechanism with linkages labeled.

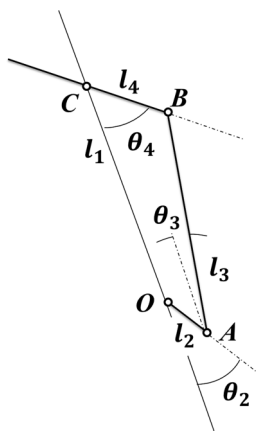

Fig. 3. Four-bar linkage mechanism for left wing.

is shown in Fig. 4 and features a simple bar and slider operated by the output shaft l_4. As l_4 rotates about point C, its end contacts and slides along l_5, which is independently hinged at point E. This motion results in a large amplification of l_5 to ± 60 deg. The final output flap angle, ζ_L, of the modified five-bar mechanism from the input angle θ_2 can be predicted analytically using the equations derived in Ref. 18. Using the linkage lengths from the mechanism design (Table 2), the output angles of the four- and modified five-bar mechanisms were simulated, and an amplification factor of 3 can be clearly seen between the two (Fig. 5). The

Table 2. Lengths of modified five-bar mechanism components

Linkage	Length (mm)
l_1	29.7
l_2	2.54
l_3	29.0
l_4	6.35
l_5	Varies with flapping
l_{ext}	20.3
l_R	14.0

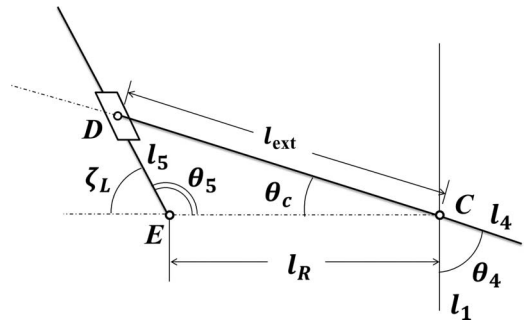

Fig. 4. Fifth bar linkage mechanism for left wing.

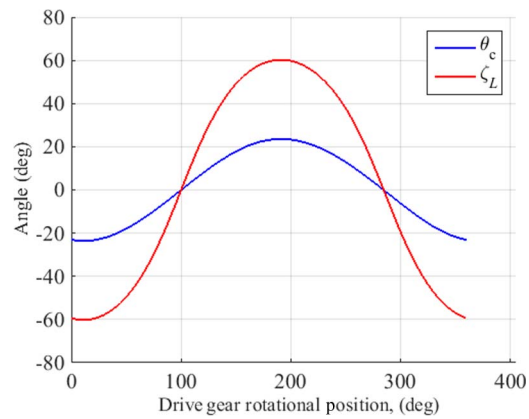

Fig. 5. Output angles of both four-bar mechanism and fifth bar in modified five-bar mechanism.

maximum flap angle from the simulation agrees well with that measured from the vehicle, which is 55 deg, with an error of ± 5 deg due to the mechanical play between l_4 and l_5.

The entire modified five-bar mechanism is machined from 6061 aluminum with steel ball bearings inserted for hinge points A, B, and C (Fig. 3). Point O is the output shaft from the drive train, which consists of a brushless dc motor and reduction gear, both selected to maximize the output torque while simultaneously minimizing its weight. An experimental approach was taken to test several motors, and the C-10 2900 KV brushless outrunner motor was finally chosen since it was found to be the lightest motor available capable of flapping the wings at a high enough frequency for liftoff. This was followed by a series of experiments to find the appropriate reduction gear to convert the low torque and high RPM output from the motor to a high torque and low RPM for flapping. After systematically varying the gear ratio from 7:1 up to 12.1:1, a reduction gear of 9.3:1 was chosen as the final design. On the current design, both

the motor pinion gear and the reduction gear were placed on the opposite side of the body as the flapping mechanism, with a shaft running through the body supported by two ball bearings. This effectively transfers only pure torque and decouples the shear loads, which are taken up by the shaft bearings (Fig. 2(a)). The motor is driven by a 10-A brushless speed controller and powered by a custom-built three-cell Li–Po battery pack, which is wired to supply the drive motor with 11.1 V and the servo actuators with 7.4 V.

Wing design and manufacturing

The wings are the most critical element of the vehicle, and therefore extensive effort was put into their design and development. They must be strong enough to withstand the inertial and aerodynamic forces experienced by the wing, but must also be as lightweight as possible to reduce inertial loads imposed at high flapping frequencies. For the present vehicle, a pair of flexible wings capable of undergoing passive deformation was chosen since flexible wings are lighter than similarly sized rigid wings and replicate biological wings much more closely (Ref. 19). Additionally, studies have shown that flapping flexible wings at insect-scale Reynolds numbers generate greater amounts of lift when compared to their rigid counterparts (Refs. 20, 21). The motion of flexible wings can be simplified kinematically down to two degrees of freedom: active flapping from the mechanism and passive twisting (since the pitch angle is a function of spanwise location) permitted by the torsional compliance of the wing and resulting from aerodynamic and inertial loading. In light of this, the wings were designed experimentally using aeroelastic tailoring by iteratively changing the wing structural components and their placement to vary the flexibility and thus the wing deformation during flapping such that the maximum amount of lift was generated. More than 50 wing designs (Fig. 6) were tested, and their performance evaluated until a final wing design was chosen that generated the most lift at the target frequency (baseline design, Fig. 7). The wings have carbon fiber leading edge and root spars fixed into a wing root made of polyether ether ketone (PEEK) plastic, a material with exceptional wear-resistant properties. It was found during testing that the leading edge spar must be as stiff as possible to limit bending in and out of the flapping plane, both of which reduce lift. A 0.8-mm foam membrane is stretched across the carbon fiber spars, so chosen since it is more flexible and also generated a lower acoustic signature than Mylar, a material often used for flapping wings (Refs. 6, 15). A free-floating cross-spar (glued to the membrane but not fixed to the wing root) was added, which aided in improving the lift generated during stroke reversal. This was because the inertial forces it generated allowed the wing to take a shape that improved its lifting capability.

It was found, however, that even this wing design required an undesirably high flapping frequency to generate the required thrust; therefore, an effort was made to improve the design. A performance goal was set at 0.32 N of lift generated per wing at 20 Hz. Frequencies much higher than 20 Hz were found to cause too much vibration onboard, and 0.32 N was half the vehicle weight. This goal was subsequently achieved and surpassed through the implementation of a flexible root shim between the wing root and root spar, much like a flexbeam in a rotor blade, which allowed the inboard portions of the wing to have a steep angle of attack (∼70 deg) relative to the incoming airstream rather than being completely vertical to it (Fig. 8). A technique was then developed to integrate the carbon fiber root spar with a flat flexible shim made of pre-preg carbon fiber, which would then be cantilevered to the wing root. Figure 7 shows the new wing design. A systematic manufacturing process was developed, which resulted in a very lightweight final wing with a mass of 0.85 g (Ref. 18). To demonstrate the repeatability of this process and to ensure similar performance characteristics between each wing manufactured, a series of six identical wings were constructed and tested. The total lift generated by each wing from 5 to 22 Hz is compared in Fig. 9. The results show strong similarity at the target frequency of 20 Hz, in which there is a maximum variation of 0.02 N of lift, or 5% variation in vertical force among the six wings.

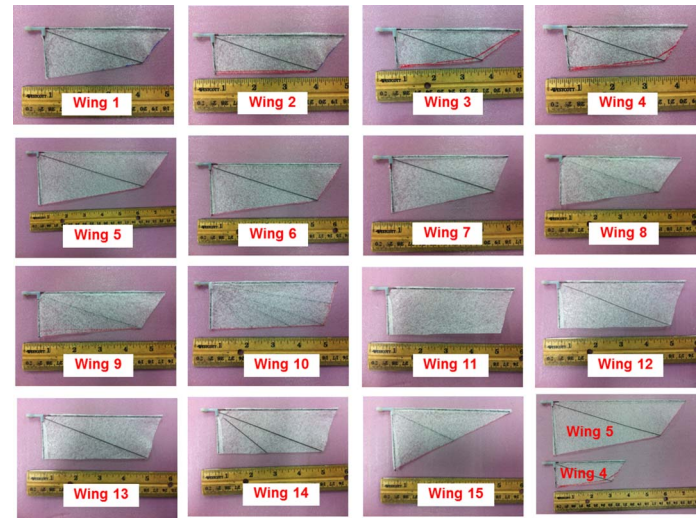

Fig. 6. Sampling of wing prototypes tested before converging on final design.

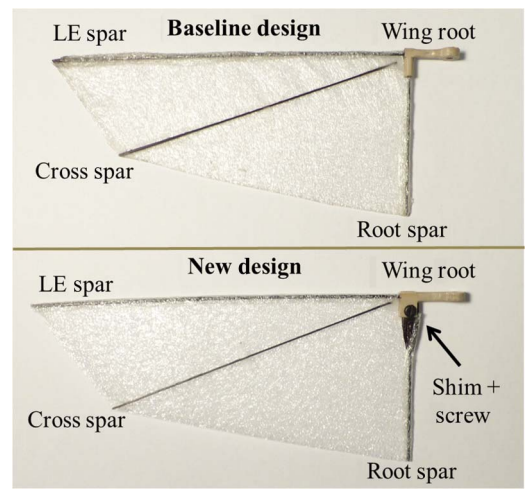

Fig. 7. Previous (baseline) design and new wing design showing flexible shim.

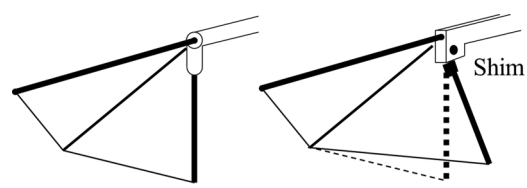

Fig. 8. Schematic of previous design in which root spar remained rigid (left) and new design featuring flexible root spar with shim (right).

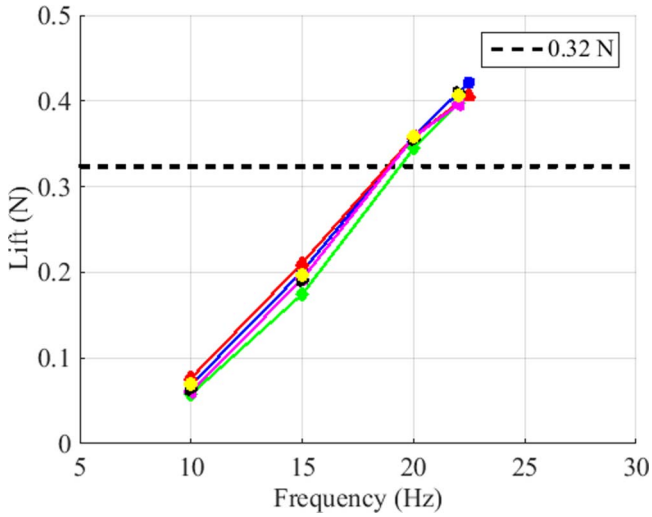

Fig. 9. Comparison plot between six wings demonstrating consistent aerodynamic performance.

Wing performance and optimization

To characterize the wing performance and converge on optimal design dimensions for the flexible shim, systematic experiments were conducted, which varied the length of the shim between the root spar and wing mount, and the thickness, in terms of layers of pre-preg carbon fiber used in constructing the shim. Varying these parameters effectively changes the stiffness of the shim, and thus the amount of flexibility and permissible deformation. Two important quantities were used in this study to evaluate each wing's performance. These were lift/electrical power and lift/f^2.

The first quantity is of interest since the electrical power required to flap the wing comes from the component of the resultant force that is parallel to the direction of motion. It is desirable to minimize this component of the force by generating a resultant force that is as vertical as possible, thereby reducing the input power required to flap the wings. The power required for flapping manifests itself in the current drawn by the motor during operation; hence it is a function of electrical power. To understand the second quantity listed above, it is important to note that as the flapping frequency is increased, the lift of a flexible wing increases due to two reasons: (1) the fact that the wing is moving faster (higher dynamic pressure) and (2) as the forces increase with frequency the passive wing twist increases and the wing starts morphing. Even though the first effect monotonically increases lift with frequency, the second effect increases lift only until the wing achieves the best shape, that is, the shape that produces the highest lift coefficient, and then decreases as the frequency increases. Thus it is important to obtain the frequency at which a wing takes the best shape, and it is important to ensure that this frequency is close to the operating frequency. Because the lift is a function of flapping frequency squared, it is necessary to divide by the quantity f^2 to remove the effect of speed and isolate the influence of wing shape on lift.

For this study, the length of the flexible shim was varied from 1 to 2 mm, and the number of carbon fiber layers used in construction of the flexible shim was varied between two and three layers. Results from these studies are presented in detail in Ref. 18, including both the variation in shim length and thickness across a range of flapping frequencies. In summary, a shim of length 1.5 mm constructed of two layers of carbon fiber performed most efficiently and was chosen as the final design.

Attitude Control and Stabilization

A two-winged flapping wing system is in general an inherently unstable system; therefore, its attitude stabilization scheme is important. Several hovering flapping wing MAVs use external control surfaces, much unlike hover-capable biological systems such as hummingbirds, which are able to achieve stability without such devices (Refs. 6, 15). The Nano Hummingbird achieves control by changing the wing slack similar to luffing a sail, which is also non-biomimetic (Ref. 11). The goal for the present vehicle, however, is true biomimicry with the greatest simplicity possible; therefore, control and stability is done exclusively by varying the specific wing kinematics during flapping.

Wing kinematics modulation

The principle of operation for wing kinematic modulation is to alter the wing-flapping plane through either tilting the plane or changing the flapping stroke amplitude of each of the wings independently. Combinations of plane tilting and amplitude modulation of each wing are used to control and stabilize the vehicle in pitch, roll, and yaw.

Pitch: A pitching moment is achieved by synchronously tilting the flapping plane of both wings either forward or backward such that there is a component of lift in the horizontal direction, H_R and H_L. Since the lift vector, which originates from the wing aerodynamic center, now no longer passes through the center of gravity (CG) of the vehicle, a moment is generated about the CG due to the force H_R and H_L acting at a vertical distance d above the CG of the vehicle. This is demonstrated in Fig. 10, which shows the outline of the original position of right and left wing planes, along with the wing planes tilted through their respective angles, β_R and β_L, to the new pitch forward positon.

Roll: Roll moment is generated by means of differential flap amplitude modulation, which changes the sweep area and thus the total lift of the wing. This technique takes advantage of the modified five-bar linkage mechanism by varying the distance between the hinge points of l_4 and l_5. This is the distance between points C and E in Fig. 3 and is denoted l_R,

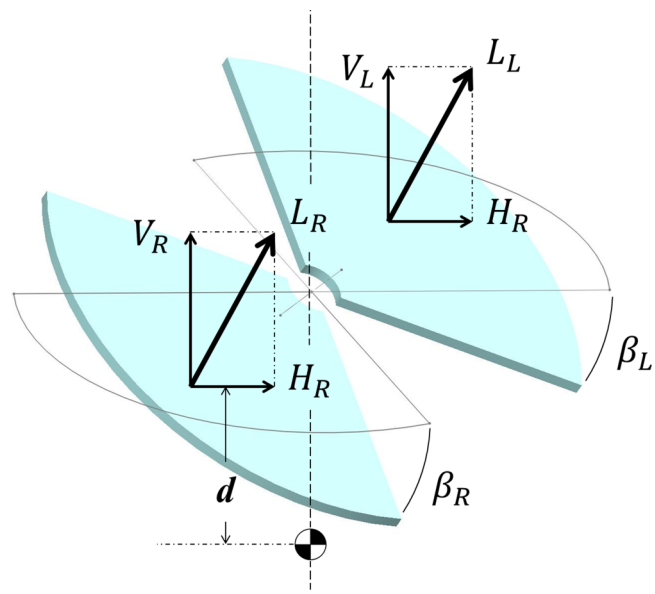

Fig. 10. Schematic of wing plane modulation for pitch stability and control.

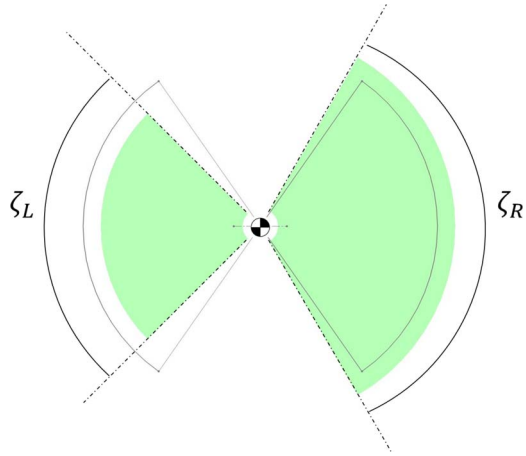

Fig. 11. Schematic of wing amplitude modulation for roll stability and control.

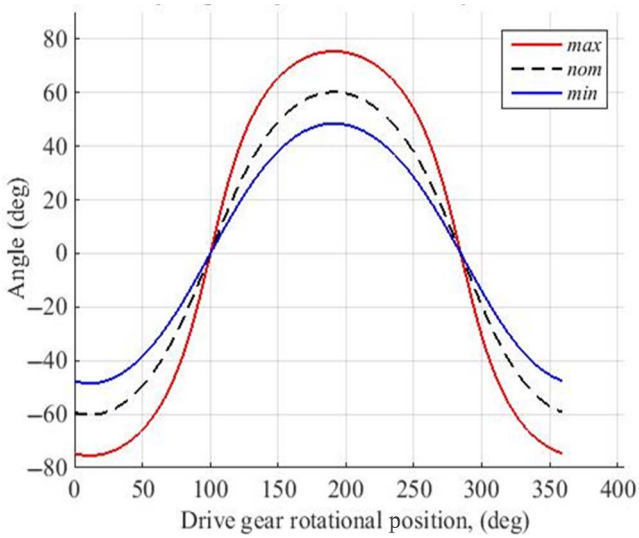

Fig. 12. Simulation of maximum and minimum flap amplitudes possible with amplitude modulation mechanism.

indicating the length of the roll trim, which varies such that for any change in roll trim for one wing, that of the other wing will change an equal and opposite amount. A schematic of the amplitude modulation is shown in Fig. 11. The original flap plane positions are outlined, along with the new lengths and amplitudes shown by the shaded region. The flap angles of the right and left wings are denoted as ζ_R and ζ_L, respectively. The maximum and minimum amplitudes that can be produced based on the physical limits of the mechanism were simulated and shown in Fig. 12. Here the zero-trim amplitude of ±60 deg as seen in Fig. 5 is shown, along with the maximum amplitude of ∼±75 deg and minimum of ∼±50 deg.

Yaw: The principle of yaw moment generation is similar to that implemented for pitching. Instead of simultaneously tilting the flapping planes in the same direction, the flapping planes are tilted differentially. The horizontal components of the lift vectors due to plane tilting are now in opposite directions, thus generating a yawing moment due to the horizontal distance between the aerodynamic center (AC) and CG of the vehicle. This is also demonstrated schematically in Fig. 13, in which the outlines of the original wing plane positions are sketched, and the new right and left wing planes are shown tilted through their respective angles, β_R and β_L.

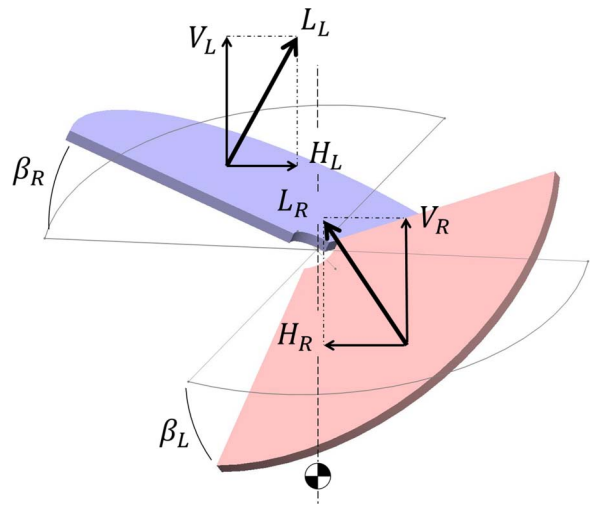

Fig. 13. Schematic of wing plane modulation for yaw stability and control.

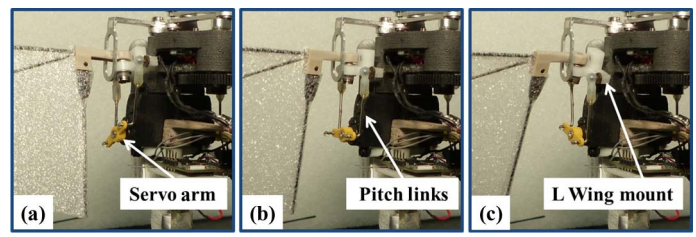

Fig. 14. Wing tilt mechanism for left (L) wing. As the servo arm rotates, the motion is transmitted via pitch links to the left wing mount, which rotates in response, effectively changing the tilt of the flapping plane.

Implementation of wing kinematics modulation

To effectively employ these modulation techniques for attitude control, simple modulation mechanisms were developed, which tilt the flapping planes and vary the amplitude as necessary for stability. There are two types of mechanisms present: the pitch–yaw mechanism for tilting the wing planes (one for each wing) and the roll mechanism for amplitude modulation. Each mechanism is independently controlled with a Power HD® DSP-33 digital microservo, which has a relatively short actuation time of 0.09 s/60° of rotation, high torque output, and minimal weight penalty. Figure 14 illustrates the pitch–yaw modulation mechanism and servo for the left wing. The servo arm rotates and transmits this motion via a set of pitch links to the wing mount, which can tilt the flapping plane, much like the motion transmitted through helicopter pitch links changes the blade angle of attack. Since the wing flaps freely on the wing mount, its plane angle being governed by the tilt of the wing mount, the angle of the lift vector can be changed as desired. The roll mechanism, as seen in Fig. 15, converts rotational motion of the servo output shaft into a linear sliding motion in the direction opposite of desired roll. This changes the length of the roll trim, l_R (Fig. 4). By moving the roll bar in the direction opposite of desired roll, l_R will increase for the wing toward which the roll bar moved, resulting in increased amplitude and thus increased lift and a subsequent roll in the opposite direction.

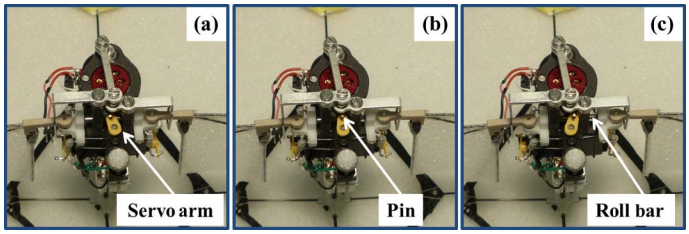

Fig. 15. Amplitude modulation mechanism. As the servo arm rotates, the motion is transmitted via the pin to the roll bar, which moves linearly in response, effectively changing the length of the fifth bar and thus the flap amplitude.

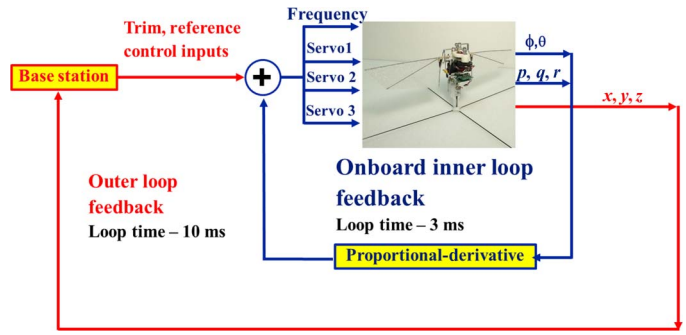

Fig. 16. Diagram of closed-loop feedback implemented in control strategy.

Autopilot

Attitude stabilization is implemented onboard using an autopilot, a custom-built embedded processor-sensor board. It weighs 1.3 g and is powered by a single one-cell 3.7 V 30 mAh Li–Po battery. The autopilot houses a STM32 microprocessor with a 32-bit ARM Cortex M3 core for high-end onboard computation tasks. The MPU-9150 IMU integrated on the board includes triaxial gyroscopes, accelerometers, and magnetometers. Wireless communications are serviced by an onboard nRF24L01 chip, a low-power 2.4 GHz radio frequency (RF) transceiver. The autopilot has a sensor update rate of 500 Hz and is capable of streaming vehicle attitude and actuator controls data to the base station with a short latency (Ref. 22). The autopilot senses the vehicle attitude and sends corrective signals to the servos for stabilization by varying the pulse width input to the servos. The full capabilities of the autopilot are described below.

Telemetry

To communicate with the onboard controller, the operator uses a LabVIEW interface through a wireless IEEE 802.15.4 data link. This connects the onboard microcontroller to the base station LabVIEW program wirelessly via a 2.4-GHz radio link. A separate wired connection between the base station and a commercially available DX6i Spectrum transmitter allows the pilot to provide roll, pitch, and yaw inputs. The base station LabVIEW program allows the operator to modify the feedback gains, change the sensitivity of pilot inputs, and record attitude data transmitted by the onboard processor. All the data processing and feedback control calculations are performed onboard by the microprocessor.

Inner-loop feedback control

The onboard gyros measure the pitch, roll, and yaw angular rates, whereas the accelerometers record the tilt of the gravity vector in the body frame. The vehicle attitude can be extracted by integrating the gyro measurements with time. However, it is known that this leads to drift in attitude measurements (Ref. 23). Accelerometers, on the other hand, offer stable bias, but are sensitive to vibrations and in general offer poor high-frequency information (Ref. 24). Therefore, a complementary filter was incorporated to extract the pitch and roll Euler angles using a high-pass filter for the gyros (4 Hz cutoff) and a low-pass filter for accelerometers (6 Hz cutoff). The flapping vibrations were filtered out since they are sufficiently higher than the body dynamics. An onboard inner-loop feedback was implemented using a proportional-derivative (PD) controller as shown in Fig. 16. The feedback states were the pitch and roll Euler angles θ and ϕ, which have a bandwidth of 10 Hz, and the attitude rates, p, q, and r. The yaw Euler angle is not measured or stabilized, only rate-based feedback is provided to yaw, which was found to be sufficient due to the neutrally stable nature of vertical axis positioning. An outer-loop feedback capability was provided for direct human piloting and can accommodate a position-tracking system should it be implemented during later research.

Gimbal Testing

Once all the vehicle subsystems were in place, a series of gimbal experiments were conducted to observe the behavior of the vehicle in a controlled setting and establish a level of stability before moving to free-flight testing. A gimbal was constructed that allows pitch, roll, and yaw rotational degrees of freedom, and the vehicle was mounted to the gimbal at the CG location. Although the vehicle demonstrated stability on the gimbal and provided insights for trimming especially in roll, the application of these results to free flight was somewhat limited since it was necessary to flap much lower than the operational frequency because of the constraining forces imposed by the gimbal. These constraints arise from the fact that the CG is held stationary from the gimbal instead of being able to move under vibratory loads during flapping. This is analogous to applying an impulse force to an object constrained against a wall versus applying the same force to an object free to move backward from the impulse. Tests were thus performed at a lower frequency for safety of the vehicle since the potential for physical damage or mechanical failure increased if these constraint forces became too large.

Flight Testing

For flight testing, a 2.4 m × 2.4 m × 2.4 m safe enclosure was constructed out of square aluminum 80-20 members and the sides were covered by a 90-μm-thick plastic sheet to retain the vehicle during flying and offer a soft impact should the vehicle collide with the walls. Additionally, a sheet of plastic was suspended from the edges of the frame a few inches off the ground to protect the vehicle in the case of a crash landing.

For a flight test to be successful, the vehicle must be in proper trim, and the closed-loop feedback control gains must be tuned. Only proportional and differential gains were used to minimize the number of variables to tune for initial flying, and because other nontraditional flying platforms have been successfully flown without integral gains (Ref. 25). Finding and maintaining these required values is difficult, must be redone after mechanical failures, and must be constantly updated due to imperceptible physical changes that the vehicle undergoes during flight. Because a given set of trim and gain values found that generate a stable flight, may, over the course of a few flight tests, cause the system oscillations to diverge, mechanical reliability and robustness is of paramount importance to minimize system variation with time.

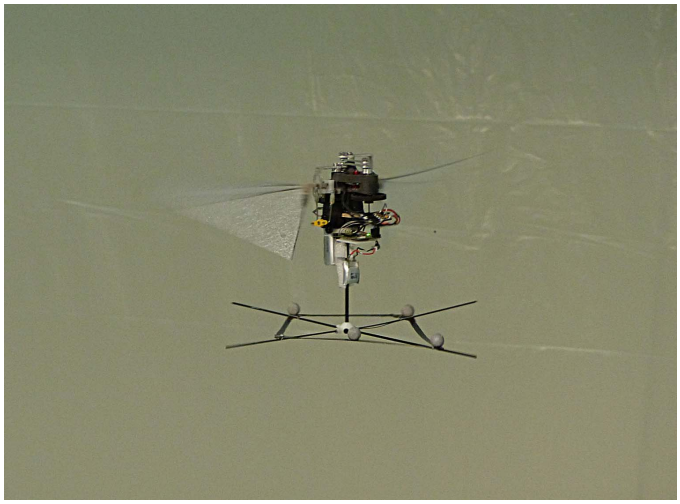

Fig. 17. Successful flight testing of the hover-capable robotic hummingbird resulting from extensive trimming and feedback gain tuning.

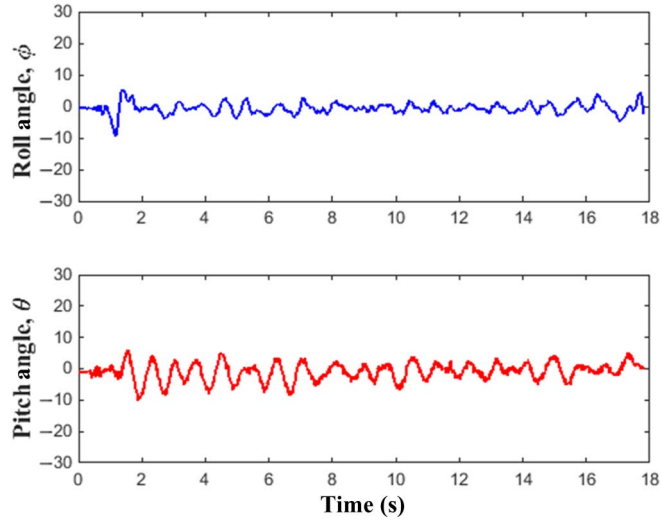

Fig. 18. Euler angles during 18-s flight test showing a maximum of ±10° variation.

A methodical approach must be taken to finding trim and gain values quickly and efficiently, and the best method found for achieving this generally involves first trimming the vehicle without the PD controller, then turning it on and determining gain values. For trimming, the vehicle is flown in short hops, its behavior is observed using a high-speed camera to capture the fast system dynamics, and trim is introduced so as to ensure liftoff is as vertical as possible, indicating that the magnitude and direction of both the lift vectors is as similar and vertical as possible. To trim roll, the amplitude of the wings is adjusted differentially to eliminate rolling moments, and to trim pitch, the angle of the flapping planes is tilted either forward or backward and held there. This can introduce a translational velocity from the horizontal component of lift, so an alternative method, and more effective, is to shift the longitudinal location of the CG relative to the AC until the CG is directly under the AC and pitching moments are eliminated. This shift can be accomplished by either repositioning the battery pack on board the vehicle or changing the length of l_3 by a small amount to shift the flap stroke mean. Once roll and pitch have been effectively trimmed and the lift vectors are as vertical as possible, the wing flap planes can be tilted differentially to provide a countertorque for yaw trim if needed.

Once the required trim values are obtained, the PD controller is turned on and the gains are determined. The fast system dynamics prevent the use of the popular Ziegler Nichols incremental approach to finding gain values, as this technique requires observing the system in motion for a lengthy time period relative to the actual amount of time this vehicle is in the air before going unstable. Additionally, owing to the inherent instability of the present system, divergent oscillations do not clearly indicate whether the gain values are too high or too low. Therefore, the method established for finding the gain values involves steadily increasing roll, pitch, and yaw differential gains until the vehicle reaches a steady-state oscillation in flight. At this point, the differential gains are decreased by 10–15%, and proportional gains are introduced with a value 15–20% greater than that of the differential gains.

This method has resulted in most flight tests demonstrating both stable and repeatable flight behavior (see Ref. 26 and Fig. 17). One remarkably stable flight was an 18-s test conducted in which the Euler roll and pitch angles oscillated with an amplitude no greater than ±10° during the length of the entire flight, shown in the Euler angle data, which is provided in Fig. 18. Although these results are promising, there remain some challenges to overcome to increase flight time and quality. First, since the motor and gearbox combination were so chosen on the basis that they were capable of lifting the vehicle, efficiency was not considered in their selection and motor overheating currently limits flight tests to ∼50–60 s. Therefore, motor and gearbox efficiency must be improved to increase flying time. Additionally, a larger capacity battery must be selected to increase the available current and slow the rapid decrease in battery voltage, which leads to changes in input power and difficulty associated with maintaining a constant motor RPM. Finally, the vehicle still drifts within the enclosure to some degree, possibly due to the absence of integral gains, which will be incorporated in future flight tests.

Summary and Conclusions

The goal of the present work has been to design, develop, and flight test a hummingbird-inspired, hover-capable flapping wing MAV using simple and innovative techniques for large flap amplitude generation and wing kinematic modulation. This paper describes the design philosophy and development of key vehicle systems and explains the aeroelastic tailoring techniques for optimizing the wing design. This flapping wing vehicle has demonstrated several stable flight tests using a closed-loop PD controller implemented onboard a custom-built kinematic autopilot. Some of the key conclusions from this study are as follows:

1) Owing to the large inertial and vibrational loads during flapping, it is necessary to reduce both flapping frequency and wing weight. For the 14-cm wing design on the present vehicle, the flapping frequency must be 20 Hz or less and the wing mass 0.85 g or less.

2) To improve the lifting capability of the wing, the root spar of the wing must be attached to the wing root through a flexible shim, which allows the inboard portions of the wing to have a steep angle of attack (∼70°) relative to the incoming air, instead of being perpendicular to it.

3) Since wing dissimilarities may prevent achieving required trim for hovering flight, it was important to manufacture the wings such that lifting performance varied by no more than 5% at the target flapping frequency.

4) It was critical to select actuators with the quickest response possible due to the fast dynamics and inherent instability of the system. For this vehicle, digital servos with an actuation time of 0.09 s/60° were selected and implemented.

5) It was important to ensure that the lift vectors of each wing are as vertical as possible for hovering flight. This was achieved by trimming

the amplitude and tilt of the flapping planes until the vehicle lifted off vertically without feedback gains.

6) To implement the appropriate feedback control, it was necessary to first apply high rate-based feedback until constant oscillations during flight were introduced, then reduce them by 10–15% and apply proportional gains 15–20% larger than differential gain values to reduce vehicle drift.

An important result of the present work is the fact that this vehicle, with a mass of 62 g has achieved stable hovering flight. This is a significant accomplishment since there is currently no known biological flyer or two-winged hover-capable MAV capable of hovering flight with a mass greater than 20 g. As a result of its heavier weight, the disk loading of the present vehicle is 15.6 N/m^2, slightly greater than that of other flapping platforms such as the Nano Hummingbird, which is about 12.9 N/m^2. As a comparison with biological flyers, the Rufous Hummingbird disk loading is on average 8.6 N/m^2 for hovering flight. Until now, the effort of this project has been focused exclusively on achieving stable flight, with little consideration for endurance. As a result, the maximum flight time is about a minute in comparison to that of the Nano Hummingbird, which is about 4 min; therefore, the next goal of this project is to improve vehicle flight time and quality by improving the efficiency of the electrical and mechanical systems.

Acknowledgments

The authors would like to acknowledge the following undergraduate students for their contributions to this project: Preetha Gautam, Aaron Lash, and Dylan Carter.

References

[1]Chanute, O., *Progress in Flying Machines*, Dover, New York, 1894, reprinted 1998.

[2]Vance, J. T., Faruque, I., and Humbert, J. S., "Kinematic Strategies for Mitigating Gust Perturbations in Insects," *Bioinspiration and Biomimetics*, Vol. 8, (1), 2013, DOI: 10.1088/1748-3182/8/1/016004.

[3]Dickinson, M. H., Lehmann, F.-O., and Sane, S., "Wing Rotation and the Aerodynamic Basis of Insect Flight," *Science*, Vol. 284, (18), 1999, pp. 1954–1960.

[4]Ansari, S. A., Zbikowski, R., and Knowles, K., "Aerodynamic Modelling of Insect-Like Flapping Flight for Micro Air Vehicles," *Progress in Aerospace Sciences*, Vol. 42, (2), 2006, pp. 129–172.

[5]Benedict, M., Coleman, D., Mayo, D., and Chopra, I., "Experiments on a Rigid Wing Undergoing Hover-Capable Flapping Kinematics at Micro-Air-Vehicle-Scale Reynolds Numbers," *AIAA Journal*, Vol. 54, (4), April 2016, pp. 1145–1157.

[6]de Croon, G. C. H. E., Groen, M. A., De Wagter, C., Remes, B., Ruijsink, R., and van Oudheusden, B. W., "Design, Aerodynamics and Autonomy of the DelFly," *Bioinspiration and Biomimetics*, Vol. 7, (2), June 2012, DOI: 10.1088/1748-3182/7/2/025003.

[7]Ratti, J., "QV: The Quad Winged, Energy Efficient, Six Degree of Freedom Capable Micro Aerial Vehicle," Ph.D. Dissertation, Georgia Institute of Technology, April 2011. Available at http://hdl.handle.net/1853/44695. Accessed January 12, 2015.

[8]Gerdes, J. W., Gupta, S. K., and Wilkerson, S., "A Review of Bird-Inspired Flapping Wing Miniature Air Vehicle Designs," *ASME Journal of Mechanism and Robotics*, Vol. 4, (2), April 2012, DOI: 10.1115/1.4005525.

[9]Wood, R. J., "The First Takeoff of a Biologically Inspired At-scale Robotic Insect," *IEEE Transactions on Robotics*, Vol. 24, (2), April 2008, DOI: 10.1109/TRO.2008.916997.

[10]Send, W., Fischer, M., Jebens, K., Mugrauer, R., Nagarathinam, A., and Scharstein, F., "Artificial Hinged-Wing Bird with Active Torsion and Partially Linear Kinematics," ICAS 2012 28th International Congress of the Aeronautical Sciences, Brisbane, Australia, September 23–28, 2012.

[11]Keennon, M., Klingebiel, K., Won, H., and Andriukov, A., "Development of the Nano Hummingbird: A Tailless Flapping Wing Micro Air Vehicle," Proceedings of the 50th AIAA Aerospace Sciences Meeting, Nashville, TN, January 9–12, 2012, pp. 2012–0588.

[12]Warrick, D. R., Tobalske, B. W., and Powers, D. R., "Lift Production in the Hovering Hummingbird," *Proceedings of the Royal Society, B: Biological Sciences*, Vol. 276, 2009, pp. 3747–3752.

[13]Cotton, P. A., "Body Size and the Ecology of Hummingbirds," *Symposium of the Zoological Society of London*, Vol. 69, 1996, pp. 239–258.

[14]Ellington, C. P., "The Novel Aerodynamics of Insect Flight: Applications to Micro-Air Vehicles," *Journal of Experimental Biology*, Vol. 202, December 1999, pp. 3439–3448.

[15]Zdunich, P., Bilyk, D., MacMaster, M., Loewen, D., DeLaurier, J., Kornbluh, R., Low, T., Stanford, S., and Holeman, D., "Development and Testing of the Mentor Flapping-Wing Micro Air Vehicle," *Journal of Aircraft*, Vol. 44, (5), 2007, pp. 1701–1711.

[16]Yilmaz, A., "Design and Development of Flapping Wing Micro Air Vehicle," Master Thesis, Swiss Federal Institute of Technology, Zurich, Switzerland, April 2010.

[17]Gemillion, G., Humbert, J. S., and Samuel, P. D., "Yaw Feedback Control of a Bio-Inspired Flapping Wing Vehicle," Proceedings of the SPIE Defense Security and Sensing Conference, San Diego, CA, April 24–26, 2012.

[18]Coleman, D., Benedict, M., Hrishikeshavan, and V., Chopra, I., "Design, Development and Flight-Testing of a Robotic Hummingbird," Proceedings of the 71st Annual AHS International Forum and Technology Display Meeting, Virginia Beach, VA, May 5–7, 2015.

[19]Pines, D., and Bohorquez, F., "Challenges Facing Future Micro-Air-Vehicle Development," *Journal of Aircraft*, Vol.43, (2), March/April 2006, pp. 290–305.

[20]Kang, C., and Shyy, W., "Passive Wing Rotation in Flexible Flapping Wing Aerodynamics," Proceedings of the 30th AIAA Applied Aerodynamics Conference, New Orleans, LA, June 25–28, 2012.

[21]Mountcastle, A. M., and Combes, S. A., "Wing Flexibility Enhances Load-Lifting Capacity in Bumblebees," *Proceeding of the Royal Society*, *B: Biological Sciences*, Vol. 280, 2013, 0531. Available at http://dx.doi.org/10.1098/rspb.2013.0531. Accessed January 13, 2015.

[22]Hrishikeshavan, V., and Chopra, I., "Refined Lightweight Inertial Navigation System for Micro Air Vehicle Applications," AHS Specialists' Meeting on Unmanned Rotorcraft and Network-Centric Operations, Chandler, AZ, January 20–22, 2015.

[23]Georgy, J., Noureldin, A., Korenberg, M., and Bayoumi, M., "Modeling the Stochastic Drift of a MEMS-Based Gyroscope in Gyro/Odometer/GPS Integrated Navigation," *IEEE Transactions on Intelligent Transportation Systems*, Vol. 11, (4), December 2010, pp. 856–872.

[24]Thong, Y. K., Woolfson, M. S., Crowe, J. A., Hayes-Gill, B. R., and Challis, R. E., "Dependence of Inertial Measurements of Distance on Accelerometer Noise," *Measurement Science and Technology*, Vol. 13, (8), 2002, pp. 1163–1172.

[25]Hrishikeshavan, V., Benedict, M., and Chopra, I., "Identification of Flight Dynamics of a Cylcocopter," *Journal of Aircraft*, Vol. 52, (1), 2015, pp. 116–129.

[26]https://www.youtube.com/watch?v=2FSRsCEJHbc.